Construction and Building Materials 189 (2018) 787–796

Contents lists available at ScienceDirect

Construction and Building Materials

journal homepage: www.elsevier.com/locate/conbuildmat

Influence of linseed oil on the microstructure and composition of lime and lime-metakaolin pastes after a long curing time

Cristiana Nunes [a,*], Petra Mácová [b], Dita Frankeová [a], Radek Ševčík [b], Alberto Viani [b]

[a] Institute of Theoretical and Applied Mechanics of the Czech Academy of Sciences, Prosecká 809/76, 190 00 Prague, Czech Republic
[b] Institute of Theoretical and Applied Mechanics of the Czech Academy of Sciences, Centre of Excellence Telč, Batelovská 485, CZ-58856 Telč, Czech Republic

HIGHLIGHTS

- Linseed oil imparted similar hydrophobic properties to lime and lime-metakaolin pastes.
- Linseed oil delayed carbonation and promoted the development of amorphous phases.
- Linseed oil can have a beneficial effect on the pozzolanic reaction of lime-metakaolin.

ARTICLE INFO

Article history:
Received 18 June 2018
Received in revised form 10 August 2018
Accepted 8 September 2018
Available online 17 September 2018

Keywords:
Linseed oil
Lime
Metakaolin
Carbonation
Hydration
Hydrophobicity
Amorphous calcium carbonate

ABSTRACT

This study investigates the effect of linseed oil on the microstructure of lime and lime-metakaolin pastes after 68 months of curing under controlled conditions. The hydrophobicity imparted by linseed oil to the pastes' bulk was confirmed by measuring water drops' contact angle. The results of thermal analysis, X-ray powder diffraction, and Fourier transform infrared spectroscopy showed that linseed oil significantly hindered the carbonation reaction in both lime and lime-metakaolin pastes and promoted the development of amorphous phases. The obtained results also indicated that linseed oil could foster the pozzolanic reaction in the lime-metakaolin system by stabilizing and/or promoting the development of hydration products resulting in reduced shrinkage in comparison with the reference.

1. Introduction

Aerial lime mortars and finishing coatings (paints) are known as one of the most compatible types of materials for the restoration of the historical heritage in which masonry and coatings were based on those materials [1]. Plastering and painting are amongst the most frequent maintenance activities in architectural restoration interventions. The significantly high number of publications dealing with the design of lime-based repair mortars for historical constructions reflects the need for more durable, while compatible, materials. One way to improve the durability of lime mortars and coatings is through the addition of additives, which are selected according to the functional requirements of the restoration material, e.g. [2–4]. Cases in point are water-repellents that aim at ameliorating the durability of mortars by hampering water ingress into the structures on which they are applied, e.g. [5–7]. Current research trends drive towards durability, compatibility, and sustainability in new construction and restoration sectors. In this context, natural additives are of growing interest to the scientific community, e.g. [8–12].

Natural oils and fats were one of the most common types of water-repellent additives used in mortars and coatings in the antiquity, and linseed oil is frequently mentioned in the European literature (e.g., *De architectura* by Vitruvius [13]). It is a highly chemically reactive oil because it contains a high amount of linolenic (48–60 wt%) and linoleic (14–19 wt%) acids with three and two double bonds, respectively. It is mostly used as a varnish thanks to its fast polymerization, e.g. [14]. The unsaturated triglycerides present in linseed oil polymerize by oxidation when exposed to atmospheric oxygen and also by photo-oxidation when exposed to light, forming macromolecular solid products [15]. When added to lime-based slurries, the glycerides present in the oil hydrolize when reacting with the alkaline binders. Subsequently, the carboxyl

* Corresponding author.
E-mail addresses: nunes@itam.cas.cz (C. Nunes), macova@itam.cas.cz (P. Mácová), frankeova@itam.cas.cz (D. Frankeová), sevcik@itam.cas.cz (R. Ševčík), viani@itam.cas.cz (A. Viani).

https://doi.org/10.1016/j.conbuildmat.2018.09.054
0950-0618/

groups coordinate with calcium to form insoluble calcium salts of fatty acids; their non-polar units are directed to the mortar-air interface, resulting in a water-repellent material [10].

Fatty acids are known to affect the crystallization process and the morphology of calcium carbonate from solutions [15,16], during carbonation reaction of lime slurry [17] and hydration products [18], which will consequently affect the porosity and PSD of a system. Other studies on the effect of vegetable oils on the properties of lime-based mortars have also shown alterations on the porosity and PSD between the reference and the mortars with additives, e.g. [3,19,20]. Regarding the effect of linseed oil on mortars, Čechová [21] has reported that an amount of 1 wt% of oil caused a slight reduction of porosity and pore size diameter (water and MIP) of aerial lime, natural hydraulic lime, lime-pozzolan, lime-brick dust and lime-cement mortars with three months and one year of age whereas an amount of 3 wt% of oil increased the porosity and the main pore radius. The mechanical strength generally improved with 1 wt% of oil addition, but 3 wt% reduced the strength substantially. Rovnaníková [22] studied the effect of stand oil in different concentrations (1, 5, and 10 wt%) in aerial lime mortars and observed a decrease in porosity (water) with increasing amount of oil. The compressive strength significantly increased with oil addition, but the flexural strength was reduced. In another work [23], both linseed and stand oil added in 1.5 wt% to aerial lime and lime-metakaolin mortars (using the same materials as in this study) resulted in a similar increment in porosity (water and MIP) and increment of the main pore radius after six months of curing. In general, the mechanical strength was reduced with both types of oil. Justnes et al. [10] reported negligible changes in the porosity (water) of Portland cement mortars with varying oil amounts (0.5–1 wt%) at 28 days of age, but a relevant decrease in the mechanical strength. Based on the reported literature, we can infer that some physical changes induced by vegetable oils in mortars are highly dependent on the type of oil (reactivity and amount), type of binder, mixing procedure, and mortar age, resulting in very different properties of the hardened material, namely regarding the porosity and mechanical strength. Thus, it is difficult to compare the results of different studies, namely when different types of oils and binders are used.

Linseed oil can be considered an eco-friendly alternative to synthetic (e.g., metal soaps and silanes) as a water-repellent additive for mortars and coatings since it gives comparable results [23]. The investigation of the effect of vegetable oils on the properties of aerial lime and lime-pozzolan materials is a recent field of research which has been mainly focused on the physical characterization and durability of mortars, e.g. [3,19,24,21,25]. This work aims at gaining further insights into the influence of linseed oil on the microstructural and compositional features of aerial lime and lime-pozzolan pastes. Paste specimens were used to focus the study on the interaction with the binder, responsible for the setting and hardening of mortars. As noted by Vejmelková et al. [26], Central Europe lacks natural pozzolans, and a possibility to obtain artificial pozzolans in the Czech Republic is the calcination of clay shales. The so-called 'burnt Czech clay shale' [26], henceforth designated as metakaolin, was selected as the pozzolanic material for this study. Regarding the composition of the specimens with oil addition, one of the objectives of this study was also to try to detect calcium salts of fatty acids, which are theoretically formed when oil reacts with the alkaline environment of the paste, as described previously. To our knowledge, calcium salts of fatty acids have been only detected in ancient samples of lime and tung oil pastes which were fully carbonated [12]. Therefore, we expected to have better chances of identifying the calcium salts having the samples matured after a long curing period. This is also the reason why we added a significantly higher amount of linseed oil (9 wt% in respect to the weight of binder) than that which has been found to be sufficient (1 to 3 wt%) to impart water-repellency to lime-based systems and achieve higher durability in comparison with the references [21,24,27]. We believe that this research is the first attempt to characterize the effect of linseed oil on the microstructure of lime and lime-metakaolin pastes.

2. Experimental

2.1. Materials and specimen preparation

The specimens were prepared in the lab with an industrially produced hydrated lime powder class CL90 (Čerták), metakaolin (Mefisto L05), and raw linseed oil (GRAC s.r.o.). According to the analysis performed by Nežerka et al., 2014 [28] on the same binders used in this study (same producer), the lime used is of high purity (98.98 wt% CaO + MgO) and the metakaolin is mainly composed of SiO_2 (52.1 wt%) and Al_2O_3 (43.4 wt%). The grading analysis showed that the predominant particle diameter in lime is 15 μm; 50% of the cumulative volume corresponds to a particle diameter of 13 μm and 90% to 38 μm; the specific surface area is 16.5 m^2/g. In the case of metakaolin, 50% of the cumulative volume corresponds to 4 μm and 90% to 11 μm; the specific surface area of metakaolin is 12.7 m^2/g [28]. Dry lime hydrate was preferred to lime putty to have more precision in the weight measurements because the water content in lime putty can vary substantially. The composition of the specimens is given in Table 1. The oil was added in the mass ratio of 1:0.1 (lime:oil); this ratio corresponds to 9 wt% of oil with respect to the binder weight. A water/binder ratio of 1.06 was used to prepare all pastes. The consistency of the fresh paste determined with the modified Vicat apparatus according to ASTM C110 [29] in triplicate is also given in Table 1.

In the case of the lime-metakaolin specimens, the dry components were first hand-mixed for 3 min with a spoon. Linseed oil was mixed with the dry components as follows: i) weighing the oil in a cup, adding a small portion of the dry component (ca. 5 g), and hand-mixing with a spoon for 2 min to obtain a homogeneous paste; ii) adding a small portion of dry component as in the first step and mixing for 2 min; iii) adding the double of the previous amount of dry component and mixing for 2 min; iv) sieving the resulting mixture with a mesh of 500 μm and mixing the retained clusters with a similar amount of dry component used in the first step in a mortar and pestle and repeating this procedure until no more clusters remain in the sieve; v) gently stir the oil-powder mix with the remaining dry portion for 3 min. The dry mixes were then hand-blended for ca. 3 min with a pre-determined amount of water necessary to achieve suitable workability for preparing paste specimens while keeping the water/binder ratio as low as possible to avoid cracking due to shrinkage during curing. The consistency of the pastes was reduced with linseed oil addition because oil reduces the adsorption of water to the binder particles. Nevertheless, the workability of the pastes with linseed oil, when worked out with a baker's knife while preparing the specimens, was better, probably because of bubble development during mixing, as described in Section 3.2, and possibly increased viscosity.

The fresh pastes were molded in rings with an inner diameter of 70 mm and a thickness of 10 mm. The geometry of the specimens was chosen based on previous experience with standard prismatic specimens used for mortar preparation in which more than 50% of the prismatic specimens fractured during curing. On the other hand, cylindrical flat specimens, identical to those used in the water vapour permeability test for mortars [30], did not fracture, probably because the cylindrical shape and lower thickness reduces corner effects and stress development during water evaporation in the early stage of curing. Moreover, the hardening reactions are also supposed to progress more homogeneously in cylindrical specimens in comparison to prismatic ones. Hence, we decided to prepare cylindrical samples instead of the prisms usually used for most of the standard evaluation tests for mortars.

During the first seven days, the pastes were kept inside the molds at 90 ± 5% relative humidity (RH) inside closed boxes at room temperature. This was mainly done with the purpose of facilitating de-moulding the specimens because after this period the paste is slightly more consistent as a consequence of some limited evaporation. After this period, the pastes were de-molded and left to cure over grid-lined shelves in a room with 60 ± 10% RH, 20 ± 5 °C, and 500 ± 50 ppm of atmospheric CO_2. The selection of the curing conditions was based on the average RH of the ambient air in the Czech Republic during the construction/repair activity period (April-September) which is between 60 and 70% [31]. Therefore, 60% RH was chosen as being representative of the on-site conditions from the beginning of the curing

Table 1
Composition by mass and resulting consistency of the fresh paste.

Specimen	Materials	Ratio	Consistency (mm)
L	Lime	–	20 ± 2
LO	Lime:Oil	1:0.1	16 ± 3
LM	Lime:Metakaolin	0.75:0.25	21 ± 3
LMO	Lime:Metakaolin:Oil	0.75:0.25:0.1	18 ± 4

process. Though a higher level of RH would favour hydraulic reactions in the lime-metakaolin system, we aimed at attaining results about the microstructure of both types of pastes under the same conditions, regardless of their composition.

A thick film of linseed oil was poured into a vessel and also left to age for the same time in the same room, which had no natural or artificial light exposure, to study its composition after polymerization and better identify its reaction with the pastes' components. The specimens were cured for 68 months before testing. The disk specimens were sliced, and one of the slices was sprayed with phenolphthalein solution [32]. The solutions remained colorless suggesting carbonation in the entire specimens' thickness.

2.2. Methods of analysis

2.2.1. Pore size distribution

The pore size distribution (PSD) was obtained using a mercury intrusion porosimeter (MIP) (Quantachrome Poremaster® PM 6013) on two replicates for each paste. The following Hg parameters were set: contact angle = 135°; surface tension = 0.485 N/m; and density = 13.534 g·cm^{-3}. Low pressure testing ranged from 1 Psi to 50 Psi and high pressure analysis from 40 Psi to 30,000 Psi.

2.2.2. N_2 physisorption analysis

Nitrogen physisorption was performed with a Micromeritics device (ASAPTM 2020) using one specimen of each paste. The specific surface area (SSA) was determined with the Brunauer–Emmett–Teller method [33]. The PSD was derived by the Barrett–Joyner–Halenda (BJH) procedure [34].

2.2.3. Wettability

The contact angle of the pastes with water was used to measure the wettability of the pastes. A drop of 0.20 ± 0.05 μl of water was poured from 50 mm distance from the surface of the paste, and a photograph was taken with a binocular microscope within 10 s after the drop hit the surface. The angle of the drop of water in relation to the surface was then calculated through image analysis by randomly selecting three points defining the drop edge in relation to the surface. Three measurements were performed for each paste.

2.2.4. Thermogravimetric analysis

The carbonation and hydration reactions in the pastes were studied with thermogravimetric analysis (TG) with a TA instrument (SDT Q600 TGA/DSC) in a static nitrogen atmosphere at a T range of 20–1000 °C and at a heating rate of 20 °C/min.

2.2.5. X-ray powder diffraction

The mineralogical composition of the samples was studied by X-ray powder diffraction (XRPD). XRPD data were collected with a Bragg–Brentano θ-θ diffractometer (Bruker D8 Advance, Cu radiation) equipped with a LynxEye 1-D silicon strip detector. The powdered specimens were side-loaded on an Al sample holder. The angular range 4–82° 2θ was covered at virtual steps scan of 0.0102° 2θ with 0.4 s/step counting time at 40 kV and 40 mA. Quantitative phase analysis, including both amorphous and crystalline fraction, was performed with the Rietveld method by spiking the sample with 10 wt% of internal standard (NIST SRM 676a alumina). Rietveld refinements have been accomplished with the TOPAS 4.2 software (Bruker AXS).

2.2.6. Fourier-transform infrared spectroscopy

The composition of the specimens was studied with attenuated total reflection Fourier-transform infrared spectroscopy (FTIR) on powdered samples at 4 cm^{-1} resolution in the spectral range 4000–650 cm^{-1} using an external module iZ10 of Nicolet iN10 spectrometer equipped with a DTGS detector, KBr beamsplitter and a Smart iTR accessory with diamond crystal. Spectra of fresh and 68-month polymerized oil were also obtained under the same conditions and used as a reference.

2.2.7. Raman spectroscopy

The Raman measurement was performed on the LO sample using micro-Raman DXR microscope (Thermo Scientific) equipped with 532 nm laser and high-resolution grating (1800 lines/mm) using a laser power of 10 mW. Each spectrum was collected as the sum of 100 scans with 4 s counting time in the spectral range 1800–50 cm^{-1} and 2 cm^{-1} spectral resolution.

2.2.8. Scanning electron microscopy

Photomicrographs of a freshly fractured surface of each paste specimen were taken with a scanning electron microscope (SEM) to investigate the effect of oil on the morphology of the pastes. The samples were sputter-coated with gold before the analysis with a MIRA II LMU (Tescan) microscope. The photomicrographs were taken under high vacuum conditions at 15 kV voltage and at a working distance of 15 mm.

3. Results and discussion

3.1. Porous structure, SSA, and wettability

Table 2 lists the pastes' open porosity and main pore radius determined with MIP, SSA, and the contact angle with water. The addition of linseed oil to the lime paste increased the porosity significantly (ca. 20%). A relevant increase of porosity (26%) was also registered for the paste with the substitution of 25 wt% of lime by metakaolin (LM). However, the addition of oil to LM mixture induced a porosity reduction of ca. 5%. The pore size distribution curves of the pastes are given in Fig. 1. All pastes show a unimodal distribution and the pastes with oil show similar curve shapes to those of the references. In the lime paste, the pore volume maximum is located at ca. 0.62 μm, whereas LO paste shows the maximum at 1.11 μm. This difference in pore size and open porosity can be mainly attributed to the lower degree of carbonation in LO as shown by TG, XRPD, and FTIR because porosity and pore size is reduced during carbonation [35]. In contrast, the pore volume maximum of LMO is slightly lower than that of LM (0.77 and 0.73 μm, respectively); this is likely to be related to the changes induced by oil in the microstructure and phases formed in each paste as further presented in Section 3.2.

Regarding the BJH porosity (Fig. 2), oil caused a slight porosity increment accompanied by a slight shift to lower pore size diameters in both L and LM pastes. These results are at odds with the slight changes registered within the corresponding pore size region (i.e., below 100 nm) with the MIP technique, but the BJH method should be more precise to detect pores in this size range. The increment of the microporosity in LMO paste can be attributed to the development of CSH phases as proposed by Espinosa and Franke [36] and confirmed by the SEM observations presented in Section 3.2. In the case of LO, the higher microporosity than the reference can also be related to the lower degree of carbonation.

Paste LO has higher SSA than the reference (ca. 14%). The SSA of lime pastes is known to decrease with the carbonation progress and is associated with the reduction of the smallest pores in the system as crystallization of $CaCO_3$ takes place [35]. The results of TG, XPRD, and FTIR presented in Section 3.2 show that LO is less carbonated than L paste, which explains the higher surface area of LO. The higher SSA of LM in comparison with L paste is attributed to the pozzolanic reaction. The surface area of LMO is similar to that of LM, though a higher amount of hydrates seems to be formed in LMO paste, as discussed in Section 3.2. The BET surface area increases with increasing amount of hydrates formed, but at later ages of hardening, the pore network of hydrates can become inaccessible to N_2, so both the values of BET surface and BJH pore size distribution may no longer correlate well with the degree of hydration [37].

The values of the contact angle of water drops on the pastes' surface reveal the hydrophobicity imparted by linseed oil to LO and LMO as the angle is significantly higher than 90°. The reference pastes absorbed the water drops after ca. 5 s after pouring.

3.2. Morphology and composition

The thermographs of linseed oil (fresh and aged) and of the pastes collected with TG are depicted in Fig. 3. The main process of the decomposition of oil (both fresh and polymerized) is observed within the temperature range from 320 °C to 510 °C, in which oil loses 97% and 79% of its weight in fresh and polymerized state, respectively. Exposition of oil to air leads to the formation of oxygenated structures [14] which results in a broad band between ca. 200 °C and 300 °C in the polymerized oil TG curve (Fig. 3a). Regarding the pastes with oil, the peaks at ca. 340 °C, and 420 °C

Table 2
Results of measured physical properties of studied pastes' mixtures.

Specimen	Porosity MIP (%)	Main pore radius (μm)	SSA- BET (m^2/g)	Contact angle with water
L	48.7 ± 1.0	0.62	8.29	n.a.
LO	58.3 ± 1.2	1.11	9.48	125° ±3
LM	61.2 ± 0.5	0.77	11.91	n.a.
LMO	58.2 ± 0.1	0.73	11.92	123° ±3

n.a. – no angle, i.e. immediate absorption.

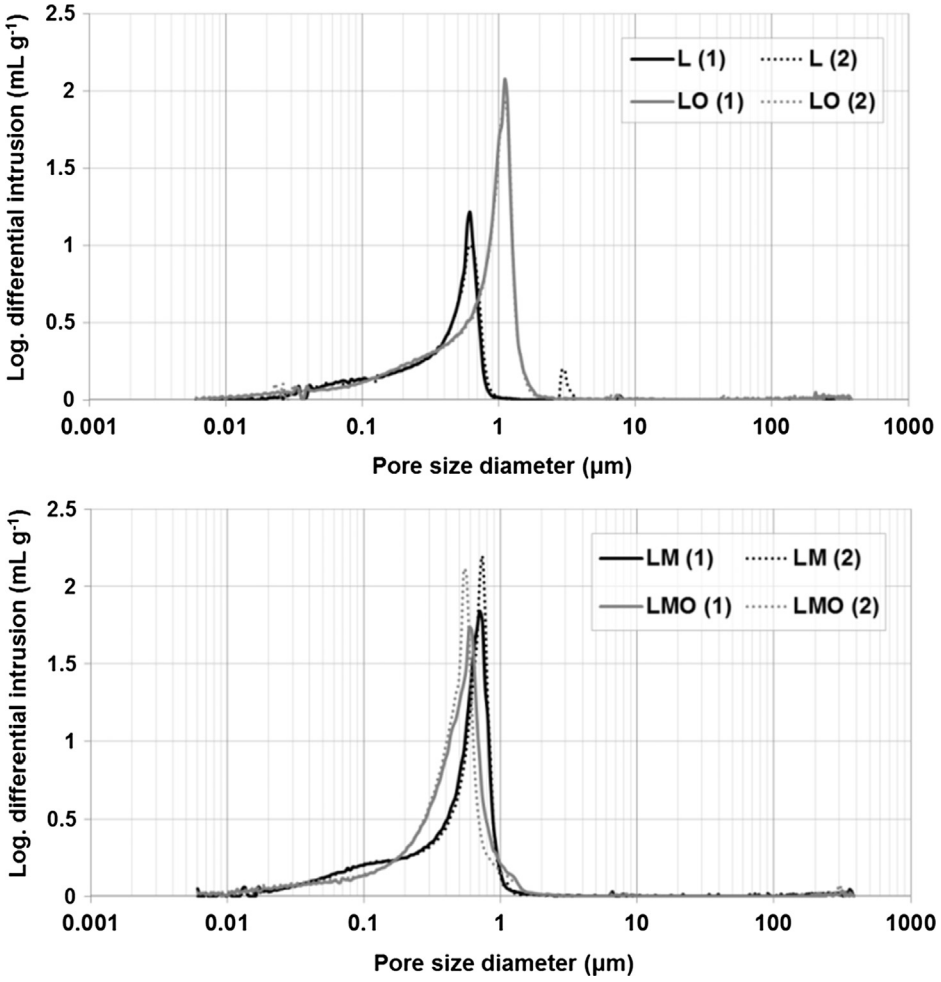

Fig. 1. Pore size distribution curves of the pastes determined with MIP: a) Lime pastes; b) Lime-metakaolin pastes.

are probably attributed to oxidation of unsaturated fatty acids in linseed oil [14,38]. The peak at ca. 455 °C indicates the presence of portlandite; this peak is partially overlapped with that of the fatty acids' oxidation peak, but it is possible to distinguish a higher amount of portlandite in LO in comparison with the reference (Fig. 3b). Correspondingly, the carbonated fraction is higher in L paste (peak between ca. 700 and 800 °C). In LO, this peak is slightly shifted to a lower temperature and partially overlaps with a peak at ca. 715 °C; we believe that this temperature dispersion in the thermographs can correspond to the decomposition of calcium carbonate with different particle size, but further studies should be performed to unveil this assumption.

The incomplete carbonation of L paste can be related to either premature drying or to hindering of CO_2 diffusion by the precipitated calcium carbonate at the specimens' surface [39]. Arandigoyen et al. [40] studied lime-pastes with different water/binder ratios (from 0.8 to 1.3) under identical curing conditions; after 2 years of curing, all the samples were completely carbonated. Hence, the amount of available water should not be the limiting factor for achieving complete carbonation of the lime paste in this study. However, the total porosity (MIP) of the samples prepared by Arandigoyen et al. was significantly higher than the value determined in this study (14% higher in the sample prepared with an identical water/binder ratio). This significant porosity difference can be related to the type of specimen and preparation technique: Arandigoyen et al. prepared cylindrical samples with a higher thickness (34 mm) and a lower diameter (40 mm), which probably resulted in less compacted specimens compared to those prepared in this study. The high compaction of the specimens probably leads to the detected lower porosity that contributed to the inhibition of CO_2 diffusion throughout the sample matrix, simultaneously engendering the development of a carbonated skin at the surface, thus further hindering CO_2 diffusion.

The carbonation delay caused by linseed oil has also been observed in previous studies conducted with mortars [24,21,25] and has also been reported in studies with other vegetable oils

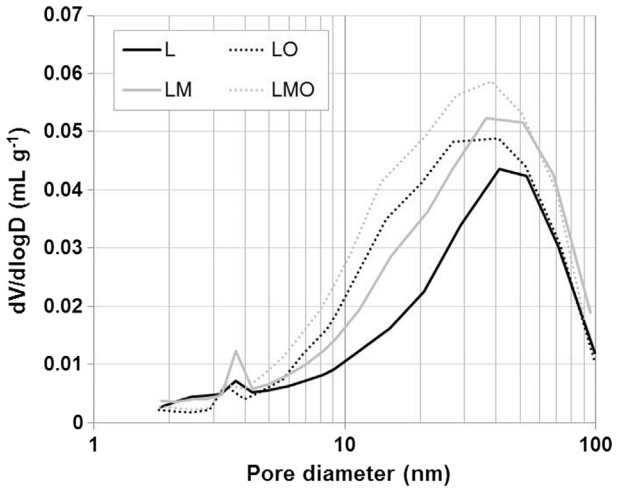

Fig. 2. Pore size distribution curves of the pastes determined with the BJH method.

added to lime-based mortars [19,20]. The carbonation delay could be attributed to the reduced contact of CO_2 with calcium hydroxide in the liquid-solid interface due to the high surface tension between the pore water transporting CO_2 and the water-repellent matrix. Amorphous calcium carbonate (ACC) hydrated phase precipitates at the initial stage of carbonation, but due to its high solubility, it rapidly transforms into calcite, which is the most stable phase under ambient conditions [39]. The presence of ACC can be detected with TG at ca. 95 and 160 °C as a result of water release [39,41]. Other authors reported that amorphous calcium carbonate could also contribute to the weight loss in the range 150–300 °C [42], this difference being probably related to the different bonding of water molecules to calcium carbonate. Hence, the broad peak in LO around 160 °C can be assigned to amorphous hydrated calcium carbonate. Kevern [8] studied the properties of Portland cement mortars with soybean oil and reported that oil significantly reduced moisture loss during curing compared to the reference mixture. Čechová [21] assumed that oil promoted moisture retention in the mortar matrix from porosity evolution results. We may thus infer that the presence of amorphous hydrated calcium carbonate in LO can be a result of moisture retention because oil introduces hydrophobicity into the system, thus slowing down the release of water during curing. The moisture retention phenomena in LO paste can also have contributed to the carbonation delay, the excess water preventing CO_2 from reacting with calcium hydroxide [35].

LMO also shows a lower carbonated fraction in comparison with LM. Similarly to LO, the signal of portlandite dehydration overlaps with that of the fatty acids' oxidation peak (Fig. 3c). LM does not contain portlandite, which seems to have been mostly consumed in the carbonation reaction. The weak peak at ca. 245 °C in LM is probably assigned to one of the hydrated aluminate phases formed by the interaction of calcium hydroxide with alumina present in metakaolin (stratlingite) [39]. LMO thermograph shows a broad peak between 95 °C and 150 °C, which can also be observed with very low intensity in LM. The presence of peaks in this temperature range in pastes with pozzolans is commonly attributed to the decomposition of CSH and calcium aluminum hydrates (CAH) [39,43] and, as mentioned above, it can also be related to partial decomposition of ACC. In LMO, the possible moisture retention imparted by linseed oil can have promoted the development and/or stabilization of hydration products thus contributing to reduce shrinkage as observed with SEM.

Table 3 reports the QPA of XRPD patterns with Rietveld refinement of the pastes and Fig. 4 shows an example of one of the refined XRPD pattern. In general, the results are in good agreement with the TG data. LO paste is less carbonated than the reference as

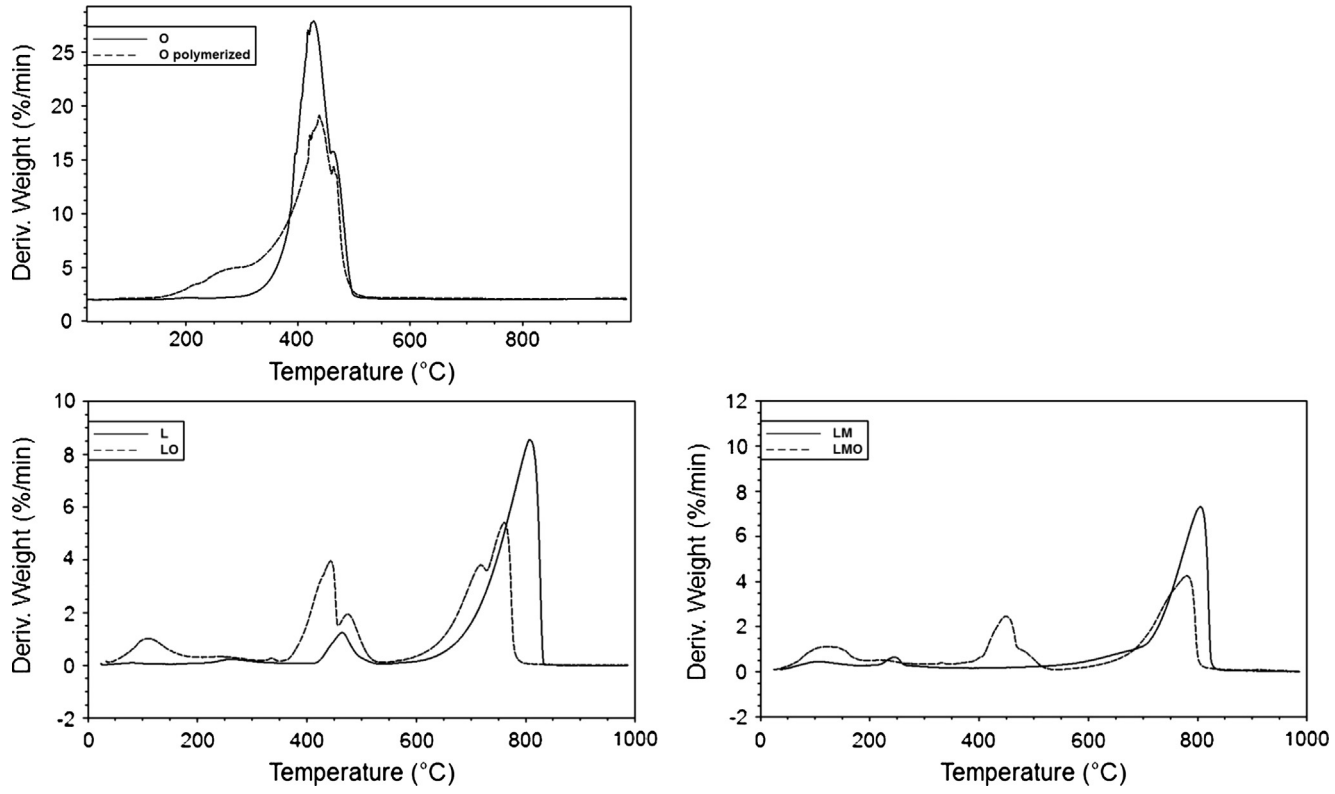

Fig. 3. Derivative thermogravimetric curves of the pastes: a) fresh linseed oil and polymerized linseed oil; b) lime pastes; c) lime-metakaolin pastes.

Table 3
Results of the QPA of XRPD pattern using Rietveld refinement of the prepared pastes.

Phase	L	LO	LM	LMO
Calcite [$CaCO_3$]	75.9	10.4	67.9	17.5
Portlandite [$Ca(OH)_2$]	10.6	37.4	n.d.	19.3
Quartz [SiO_2]	n.d.	n.d.	0.6	0.4
Mullite [$Al_6Si_2O_{13}$]	n.d.	n.d.	1.2	n.d.
Amorphous	13.5	52.1	30.2	62.9

n.d. – not detected.

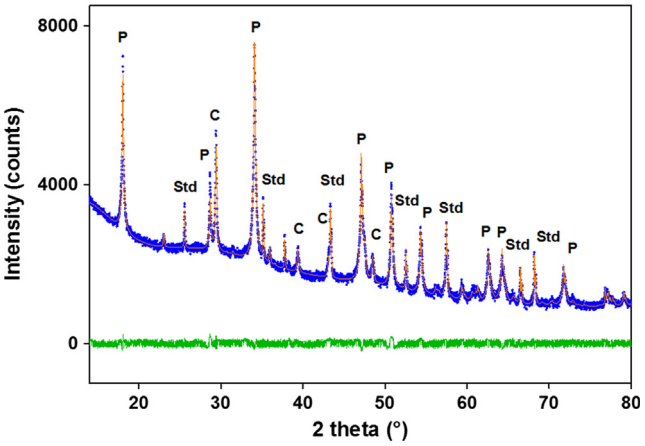

Fig. 4. Example of Rietveld refinement of XRPD pattern collected for LO paste showing the observed (blue), calculated (red line) and difference curve (green bottom line) of the refined XRPD patterns. Notation: C = Calcite; P = Portlandite; Std = NIST676a Al_2O_3 internal standard considered as component itself. (For interpretation of the references to colour in this figure legend, the reader is referred to the web version of this article.)

reflected by the higher content of portlandite. Concordantly, the calcite content in LO is significantly lower in comparison with the reference, but the amorphous content (which in these samples includes all the hydrated products) is considerably higher, thus confirming the TG and further presented SEM results. LMO also shows the presence of portlandite, significantly lower calcite content and the double amount of amorphous phase than the reference. These results are in line with a previous study conducted with mortars with 1.5 wt% of oil with six months of age in which LMO also showed considerably lower calcite content, a higher amount of amorphous phases, plus tetracalcium monocarboaluminate [27].

The FTIR spectra of linseed oil and the pastes are depicted in Fig. 5. The spectral changes between fresh and polymerized linseed oil are clearly visible: disappearance of the peak at ca. 3009 cm^{-1} ((C—H)═CH stretching vibration), decrease of the absorption at 722 cm^{-1} (isolated double bonds), appearance of a broad band centred at ca. 3412 (hydroxyl groups) and of a weak absorption at 1620 cm^{-1} attributed to the formation of conjugated double bonds. These results are consistent with those of Lazzari and Chiantore [14] who explained that hydrocarbon oxidation during drying is promoted by hydrogen atoms, hydroperoxide formation being easier on linolenic and linoleic groups. The —C═O stretching vibration at 1742 cm^{-1} in the fresh oil and between 1732 and 1708 cm^{-1} in the polymerized oil is not present in the spectra of LO and LMO samples, although this peak is most intense in the spectrum of linseed oil. The absence of this double bond reveals the reaction of the binders with oil as described in Section 1, though no calcium salts of fatty acids were identified.

The FTIR spectra of the pastes confirm the presence of portlandite in the specimens with oil shown by the peak at

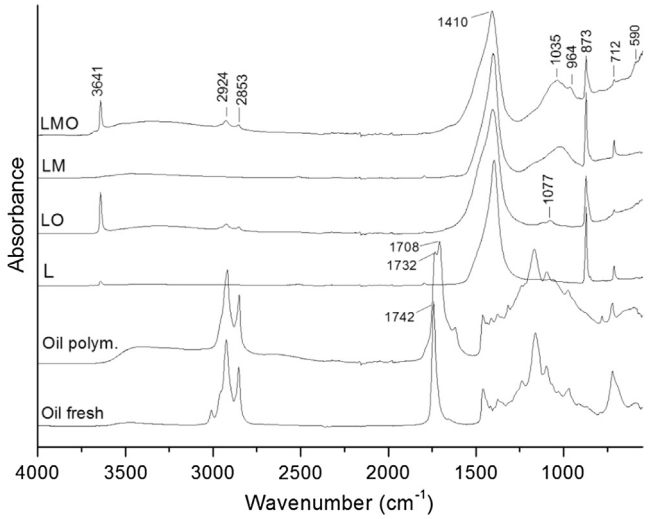

Fig. 5. FTIR spectra of the pastes and linseed oil.

3641 cm^{-1} (O—H stretching vibration). The presence of calcite can be detected by the peaks at 712 cm^{-1} (in-plane bending), 873 cm^{-1} (O-C-O out-of-plane bending), 1410 cm^{-1} (asymmetric stretching) and 1077 cm^{-1} (C—O symmetric stretching) [44]. The peaks related to calcite are more intense in LM than in LMO, confirming the TG, XRPD and further discussed SEM observations. Such results are consistent with the decalcification of hydrated phases in LM. The bands assigned to metakaolin are revealed by a broad band at ca. 1035 cm^{-1} related to Si—O stretching vibration and at ca. 590 cm^{-1} related to Si—O bending vibration; the shoulder at ca. 964 cm^{-1} observed in LMO could be ascribed to CSH [45]. The metastable calcium carbonate polymorphs, aragonite, and vaterite were not detected in our samples. Nonetheless, it is known that these polymorphs can be formed in different mortars where linseed oil was used as an additive [27,46]. As reported in Jiang et al. [17], only calcite was observed to be formed during the carbonation of lime slurry in the presence of long chain fatty acids, which strongly influenced the morphology of calcite particles.

Raman spectroscopy confirmed the presence of amorphous calcium carbonate (ACC) in LO paste (Fig. 6); calcite (C) peaks are seen at 1086, 712, 281 and 154 cm^{-1}, portlandite (P) is identified by the broad band at ca. 680, 357, and 255 cm^{-1}, and ACC by the peak at 1080 cm^{-1}, and by the broad band at ca. 720 cm^{-1}. Given that the ACC peak at 1080 cm^{-1} overlaps with that of calcite at 1086 cm^{-1}, the band assigned to ACC was detected through deconvolution of the Raman spectrum between 1140 and 1020 cm^{-1} (inset in Fig. 6) [47]. The amount of calcium carbonate calculated from the TG curve of LO was 53.4 wt%, whereas the amount detected with QPA was 10.4 wt%. These results indicate that most of the calcium carbonate present in LO paste was in the form of ACC.

Lime and lime-metakaolin pastes with oil showed the presence of large rounded pores with varying diameters from ca. 10 up to 200 μm in both types of specimens (Fig. 7). The development of this type of pores is attributed to the saponification reaction resulting from mixing oil with the alkaline components of the paste. This reaction is considered to occur during mixing with water, forming air bubbles in the paste. Such phenomenon has also been observed in a previous study with mortars with linseed oil addition and confirmed by the measured air content of the fresh mix, which was significantly higher in mortars with oil in comparison with the references [24]. The fatty acid anions resulting from the reaction of oil with the binder consist of non-polar hydrocarbon chains linked with polar carboxyl groups. The polar groups will direct to water and lower the surface tension, thus promoting the development

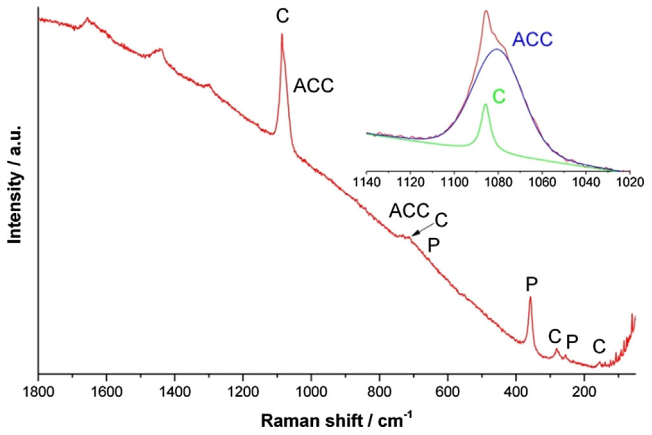

Fig. 6. Raman spectra of LO paste. The inset gives a detail of the spectrum showing Gaussian line profiles for calcite and ACC.

of air bubbles [48]. Centauro et al. [25] also observed large rounded pores in aerial and natural hydraulic lime mortars with linseed oil (2 wt%) under the optical microscope. This type of pores probably corresponds to closed pores which are neither accessible to mercury or their size is above the detection limit of the MIP technique.

The analysis of the morphology of the pastes can help in understanding the relationships between the hardening reactions and the sample microstructure. Fig. 8 shows the morphology of the lime pastes as observed under SEM. In general, the lime paste shows a finer-grained structure than LO composed of particles of small polyhedral-shaped crystals. Hexagonal plate-like crystals of portlandite were also observed in L paste, preferentially in small pores of ca. 2 μm (Fig. 8a). The matrix of LO was more porous and heterogeneous; portlandite crystals were larger and thicker, often showing sub-angular shape, and appeared in a larger amount (Fig. 8b). Fig. 9 shows details of the morphological aspects in LO observed punctually: (i) very large portlandite crystals of ca. 10 μm in size (Fig. 9a) inside the large rounded pores described previously; (ii) filamentous shaped particles resembling ACC spicules of the sea tulip *Pyura pachydermatina* (see, e.g. [49] (Fig. 9b); (iii) spherulitic particles covered with needles (Fig. 9c). The later type of morphology could be assigned to vaterite (spherule) and aragonite (needles), but XRPD and FTIR did not provide evidence of its presence, probably because of its rare occurrence in the matrix. Alternatively, the presence of fatty oils remarkably influenced calcite morphology and their dimensions [17]. The morphological alteration of $CaCO_3$ particles in the presence of carboxylic acids was also detected in work by Wada et al. [15]. In the presence of carboxylic acids during the crystallization of calcium

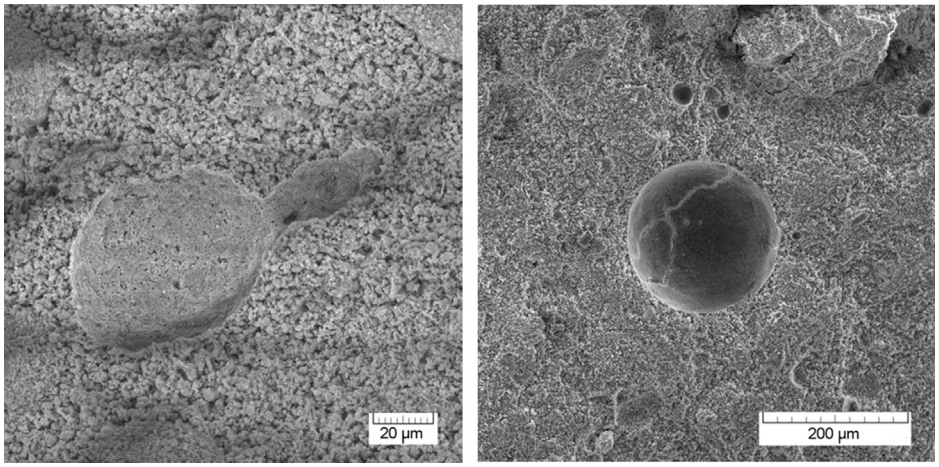

Fig. 7. SEM microphotographs showing the aspect of the rounded pores (bubble-like) developed in LO (a) and LMO (b) caused by entrained air during mixing.

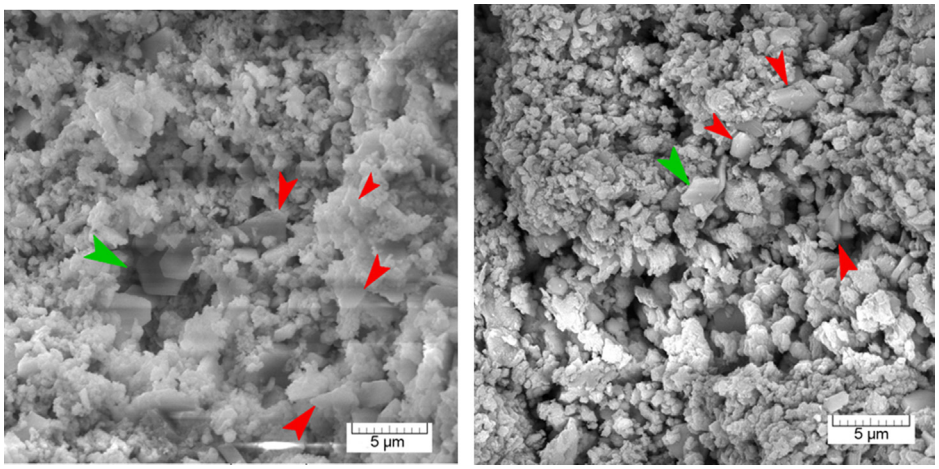

Fig. 8. SEM photomicrographs of the lime pastes: a) Aspect of the L paste showing ACC with some plate-like crystals with irregular edges (red arrows) and portlandite crystals (green arrow) formed inside a micropore; b) Aspect of LO paste showing a portlandite crystal (green arrow) and thick plate-like crystals (red arrows), probably corresponding to portlandite. (For interpretation of the references to colour in this figure legend, the reader is referred to the web version of this article.)

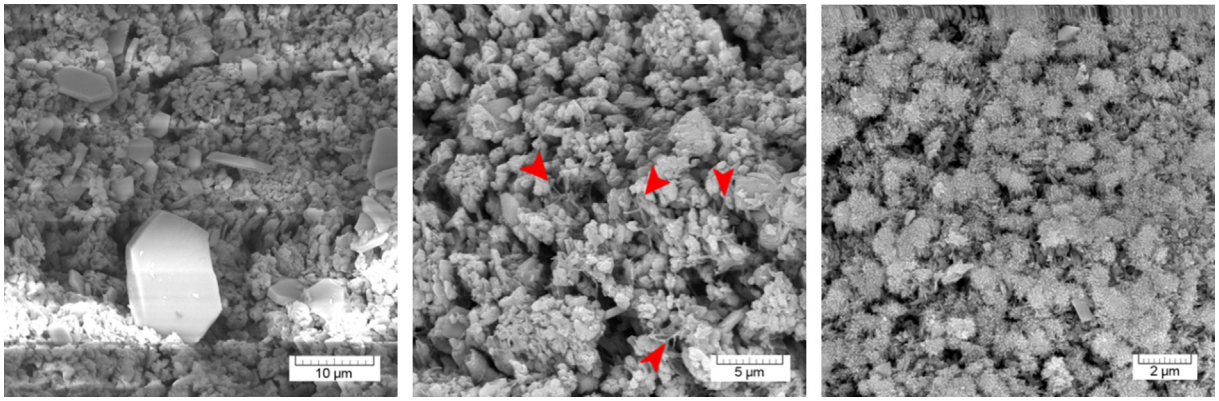

Fig. 9. SEM photomicrographs of LO paste showing large portlandite crystals formed inside a bubble-type pore (a), filamentous structures indicated by red arrows (b), and spherules covered with submicrometer-sized needles (c). (For interpretation of the references to colour in this figure legend, the reader is referred to the web version of this article.)

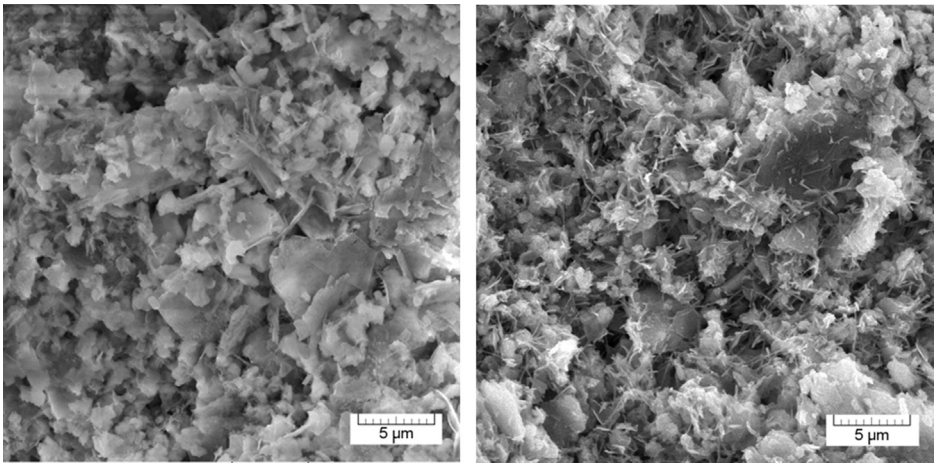

Fig. 10. SEM photomicrographs of lime-metakaolin pastes: a) Aspect of the amorphous particles and irregular-edged flakes in LM matrix; b) Aspect of the fibers and flakes intimately mixed in LMO.

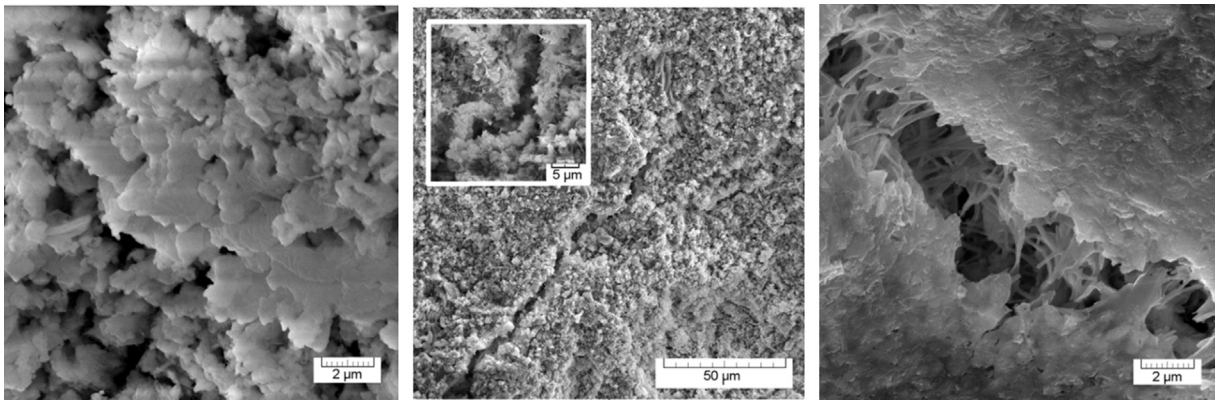

Fig. 11. SEM photomicrographs of lime-metakaolin pastes showing the typical morphology observed inside pores: a) Calcite plate-like crystals formed in LM pores; b) Crack in LM matrix – the inset shows a detail of the crack; c) Crack inside a ca. 200 μm diameter pore in LMO showing fibre-like bundles of hydrate phases connecting the crack walls.

carbonate from water solutions of $CaCl_2$ and $NaHCO_3$, calcite crystals were observed to have less regular shape (amorphous-like) morphology depending on the type of carboxylic acid. It has been shown by Jiang et al. [17] that fatty acid could be adsorbed to Ca $(OH)_2$ particles forming micelles consisting of fatty acid ions and calcium salts of fatty acids. These micelles can then act as templates for $CaCO_3$ formation and, in our case, they are probably causing hindering the carbonation of lime and preserving ACC.

Fig. 10 shows the morphology of the lime-metakaolin pastes. Both LM and LMO pastes show an amorphous texture composed of amoeboid-shaped grains and flakes with irregular edges, the latter being generally attributed to calcium silicate hydrates (CSH),

e.g. [39]. LMO paste shows smaller sized particles and a high amount of fine fiber-like bundles of CSH, which were rarely visible in LM. These observations are in line with the slight shift of the MIP pore size diameter to a lower value in LMO (Fig. 1b) and with the increment of the microporosity (Fig. 2). Similar microstructural differences were observed between LM and LMO mortars and were linked to the higher mechanical strength of LMO in comparison with LM [24]. Fig. 11 shows the aspect of the morphology inside the pores in lime-metakaolin pastes. LMO pore walls generally show smooth texture. Mainly in the largest pores (ca. 100–200 μm, see Fig. 7b), cracks (ca. 4 μm) filled with fibrous structures interconnecting the crack walls were developed (Fig. 11c). LM paste shows platelet-like particles often growing parallel to each other (Fig. 11a); this type of structure has been observed in the pure lime paste (Fig. 9b), thus probably corresponding to calcite, which was detected in a significant amount with XRPD in LM. Hydrated phases are susceptible to decalcification through carbonation reaction, causing shrinkage cracks and a decrease in strength [50]. This phenomenon was confirmed by the presence of cracks in LM paste along which, amorphous grains of what appears to be calcium carbonate could be observed (Fig. 11b). This aspect explains the high porosity value of LM paste and why the porosity is lower in LMO because oil seems to inhibit the development of shrinkage cracks, which is in line with previous research with mortars [24]. The considerably higher porosity of LO and LMO in comparison with that of L, though the presence of cracks was rare in these pastes, could be related to one of the disadvantages of the MIP technique, i.e. cracking of the matrix during high pressure mercury injection giving access channels (ink-bottle effect) to the large rounded pores described earlier (Fig. 7).

4. Conclusions

This study provides advanced insights into the role of linseed oil in the composition and microstructure of lime and lime-metakaolin pastes cured for a long time under controlled conditions. The results have important implications for applications in mortar or coating (paint) production. The main conclusions can be summarized as follows:

- The addition of 9 wt% of linseed oil to lime and lime-metakaolin imparted high hydrophobicity to the hardened pastes as reflected by the high contact angle of water drops with the surface of the specimens.
- Linseed oil significantly increased the porosity of the lime paste probably by both influencing the crystallization process during curing (leading to a high content of hydrated amorphous phases) and by air entrapment during mixing. The porosity and pore size diameter of the lime-metakaolin matrix was slightly lower than the reference, probably thanks to the higher amount of hydration products developed and to reduced shrinkage.
- The incomplete carbonation of the lime paste after a long period of curing (68 months) can be related to either premature drying or to hindering of CO_2 diffusion by the precipitated calcium carbonate at the specimens' surface. The carbonation can also have been influenced by the well-compacted type of specimen prepared as revealed by the low porosity in comparison with pastes with similar composition and water/binder ratio reported in the literature.
- Linseed oil delayed the progress of the carbonation reaction in the lime paste. The carbonation delay could be assigned to the reduced contact of CO_2 with calcium hydroxide in the liquid-solid interface due to the matrix high surface tension between the pore water transporting CO_2 and the water-repellent matrix, formation of micelles consisting of fatty acid ions and/or calcium salts, and/or to moisture retention caused by the hydrophobicity imparted by linseed oil.
- The results indicated that most of the calcium carbonate formed in LO paste corresponds to ACC, which can also be a result of moisture retention.
- The lime paste with linseed oil showed a more heterogeneous texture than the reference with the punctual formation of distinct habits (e.g., filamentous structures, rounded grains covered with submicrometer-sized needles).
- The lime-metakaolin paste was virtually entirely carbonated which indicates that the curing conditions (60 ± 10% RH, 20 ± 5 °C and 500 ± 50 ppm of atmospheric CO_2) hindered the development and stabilization of hydration products in this system.
- The available portlandite in the lime-metakaolin paste seems to have been almost completely converted into calcite. This may have been promoted by the high porosity of LM paste and by the curing conditions favouring the carbonation reaction in detriment of the development and/or stabilization of hydration phases. The future planned measurement of the moisture evolution and shrinkage during curing and testing of the mechanical properties of these pastes should help to confirm this hypothesis.

Conflict of interest

None.

Acknowledgments

This study was supported by the Czech Science Foundation; project reference 18-28142S. Petra Mácová, Radek Ševčík, and Alberto Viani acknowledge support by the project No. LO1219 under the Ministry of Education, Youth and Sports National sustainability programme I of Czech Republic. We are thankful to Veronika Koudelková for taking the SEM microphotographs, Milan Svoboda for performing the MIP and N_2 physisorption analysis, and Jaroslav Valach and Pavel Beneš for developing the program to measure the drop contact angles from photographs. We are also thankful to two anonymous reviewers who gave valuable comments to improve the clarity of the paper.

References

[1] R. Veiga, Air lime mortars: What else do we need to know to apply them in conservation and rehabilitation interventions? A review, Constr. Build. Mater. 157 (2017) 132–140, https://doi.org/10.1016/j.conbuildmat.2017.09.080.
[2] P. Zhao, M.D. Jackson, Y. Zhang, G. Li, P.J.M. Monteiro, L. Yang, Material characteristics of ancient Chinese lime binder and experimental reproductions with organic admixtures, Constr. Build. Mater. 84 (2015) 477–488, https://doi.org/10.1016/j.conbuildmat.2015.03.065.
[3] L. Ventolà, M. Vendrell, P. Giraldez, L. Merino, Traditional organic additives improve lime mortars: new old materials for restoration and building natural stone fabrics, Constr. Build. Mater. 25 (2011) 3313–3318, https://doi.org/10.1016/j.conbuildmat.2011.03.020.
[4] A. Izaguirre, J. Lanas, J.I. Álvarez, Ageing of lime mortars with admixtures: durability and strength assessment, Cem. Concr. Res. 40 (7) (2010) 1081–1095, https://doi.org/10.1016/j.cemconres.2010.02.013.
[5] A.C. Magalhães, M.R. Veiga, F. Cartaxo, Characterization of lime mortars with water repellent for use on ancient building's walls, Proc. 7th Int. Masonry Conference (7IBMAC), British Masonry Society, London, 2015.
[6] A. Izaguirre, J. Lanas, J.I. Álvarez, Effect of water-repellent admixtures on the behaviour of aerial lime-based mortars, Cem. Concr. Res. 39 (11) (2009) 1095–1104, https://doi.org/10.1016/j.cemconres.2009.07.026.
[7] P. Maravelaki-Kalaitzaki, Hydraulic lime mortars with siloxane for waterproofing historic masonry, Cem. Concr. Res. 37 (2) (2007) 283–290, https://doi.org/10.1016/j.cemconres.2006.11.007.
[8] J.T. Kevern, Using soybean oil to improve the durability of concrete pavements, J. Pavement Res. Technol. 3 (5) (2010) 280–285.

[9] H. Vikan, H. Justnes, Influence of vegetable oils on durability and pore structure of mortars, ACI 234 (2006) 417–430.
[10] H. Justnes, T.A. Ostnor, B. Vila, Vegetable oils as water-repellents for mortars Chiang Mai, in: Proc. 1st Int. Conf. Asian Concrete Federation, 2004, pp. 689–698.
[11] R. Ravi, M. Rajesh, S. Thirumalini, Mechanical and physical properties of natural additive dispersed lime, J. Build. Eng. 15 (2018) 70–77, https://doi.org/10.1016/j.jobe.2017.10.009.
[12] S. Fang, H. Zhang, B. Zhang, G. Li, A study of Tung-oil–lime putty – a traditional lime based mortar, Int. J. Adhes. Adhes. 48 (2014) 224–230, https://doi.org/10.1016/j.ijadhadh.2013.09.034.
[13] Vitruvius, I.D. Rowland, in: Vitruvius: 'Ten Books on Architecture, 1999, https://doi.org/10.1017/cbo9780511840951.
[14] M. Lazzari, O. Chiantore, Drying and oxidative degradation of linseed oil, Polym. Degrad. Stab. 65 (1999) 303–313, https://doi.org/10.1016/s0141-3910(99), 00020-8.
[15] L. Masschelein-Kleiner, Ancient Binding Media, Varnishes and Adhesives, ICCROM, 1995;
N. Wada, K. Kanamura, T. Umegaki, Effects of carboxylic acids on the crystallization of calcium carbonate, J. Colloid Interface Sci. 233 (1) (2001) 65–72, https://doi.org/10.1006/jcis.2000.7215.
[16] E. Loste, E. Díaz-Martí, A. Zarbakhsh, F.C. Meldrum, Study of calcium carbonate precipitation under a series of fatty acid langmuir monolayers using brewster angle microscopy, Langmuir 19 (7) (2003) 2830–2837, https://doi.org/10.1021/la026837k.
[17] J. Jiang, D. Xu, Y. Zhang, S. Zhu, X. Gan, J. Liu, From nano-cubic particle to micro-spindle aggregation: the control of long chain fatty acid on the morphology of calcium carbonate, Powder Technol. 270 (2015) 387–392, https://doi.org/10.1016/j.powtec.2014.10.047.
[18] J.F. Young, Effect of organic compounds on the interconversions of calcium aluminate hydrates: hydration of tricalcium aluminate, J. Amer. Cer. Soc. 53 (2) (1970) 65–69, https://doi.org/10.1111/j.1151-2916.1970.tb12011.x.
[19] P. Pahlavan, S. Manzi, M.T. Rodriguez-Estrada, M.C. Bignozzi, Valorization of spent cooking oils in hydrophobic waste-based lime mortars for restorative rendering applications, Constr. Build. Mater. 146 (2017) 199–209, https://doi.org/10.1016/j.conbuildmat.2017.04.001.
[20] A.F.G. Sá, Renders in walls of lime and stone (in Portuguese), MSc dissertation, Instituto Superior Técnico da Universidade Técnica de Lisboa, Lisbon, 2005.
[21] E. Cechová, The Effect of Linseed Oil on the Properties of Lime-based Restoration Mortars (PhD dissertation), University of Bologna, 2009.
[22] P. Rovnaníková, Plasters (in Czech), STOP 80-86657-00-0, Prague, 2002.
[23] C. Nunes, Z. Slížková, Lime-based repair mortars with water-repellent admixtures: laboratory durability assessment, in: R. Amoêda, S. Lira, C. Pinheiro (Eds.), Proc. 2nd Int. Conf. Preservation, Maintenance and Rehabilitation of Historical Structures, 2015, pp. 851–860. Barcelos: GLI.
[24] C. Nunes, Z. Slížková, Hydrophobic lime-based mortars with linseed oil: characterization and durability assessment, Cem. Concr. Res. 61–62 (2014) 28–39, https://doi.org/10.1016/j.cemconres.2014.03.011.
[25] I. Centauro, E. Cantisani, C. Grandin, A. Salvini, S. Vettori, The influence of natural organic materials on the properties of traditional lime-based mortars, Int. J. Architect. Herit. 11 (5) (2017) 670–684, https://doi.org/10.1080/15583058.2017.1287978.
[26] E. Vejmelková, M. Keppert, P. Rovnaníková, Z. Keršner, R. Černý, Properties of lime composites containing a new type of pozzolana for the improvement of strength and durability, Comp. Part B: Eng. 43 (8) (2012) 3534–3540, https://doi.org/10.1016/j.compositesb.2011.11.053.
[27] C. Nunes, Z. Slížková, Freezing and thawing resistance of aerial lime mortar with metakaolin and a traditional water-repellent admixture, Constr. Build. Mater. 114 (2016) 896–905, https://doi.org/10.1016/j.conbuildmat.2016.04.029.
[28] V. Nežerka, Z. Slížková, P. Tesárek, T. Plachý, D. Frankeová, V. Petráňová, Comprehensive study on mechanical properties of lime-based pastes with additions of metakaolin and brick dust, Cem. Concr. Res. 64 (2014) 17–29, https://doi.org/10.1016/j.cemconres.2014.06.006.
[29] ASTM C110 – 16e1: Standard Test Methods for Physical Testing of Quicklime, Hydrated Lime, and Limestone, Chapter 5: Standard consistency of lime putty (Modified Vicat Apparatus).
[30] EN 1015-19 (1999) Methods of test for mortar for masonry - Part 19: Determination of water vapour permeability of hardened rendering and plastering mortar.
[31] Data provided on the website of the Czech Hydrometeorologic Institute – average RH from the period 1981–2010): http://portal.chmi.cz/ (retrieved on 2018.08.08).
[32] CPC18 Measurement of hardened concrete carbonation depth, Mater. Struct. 21 (126) (1988) 453–455 10.1007/bf02472327.
[33] S. Brunauer, P.H. Emmett, E. Teller, Adsorption of gases in multimolecular layers, J. Am. Chem. Soc. 60 (1938) 309–319, https://doi.org/10.1021/ja01269a023.
[34] E.P. Barret, L.G. Joyner, P.P. Halenda, The determination of pore volume and area distributions in porous substances. I. Computations from nitrogen isotherms, J. Am. Chem. Soc. 73 373–380 (1951), https://doi.org/10.1021/ja01145a126.
[35] M. Arandigoyen, B. Bicer-Simsir, J.I. Alvarez, D.A. Lange, Variation of microstructure with carbonation in lime and blended pastes, Appl. Surf. Sci. 252 (20) (2006) 7562–7571, https://doi.org/10.1016/j.apsusc.2005.09.007.
[36] R.M. Espinosa, L. Franke, Influence of the age and drying process on pore structure and sorption isotherms of hardened cement paste, Cem. Concr. Res. 36 (2006) 1969–1984, https://doi.org/10.1016/j.cemconres.2006.06.010.
[37] I. Odler, The BET-specific surface area of hydrated Portland cement and related materials, Cem. Concr. Res. 33 (2003) 2049–2056, https://doi.org/10.1016/s0008-8846(03), 00225-4.
[38] E. Kaisersberger, DSC investigations of the thermal characterization of edible fats and oils, Thermochim. Acta 151 (1989) 83–90, https://doi.org/10.1016/0040-6031(89), 85339-0.
[39] O. Cizer, Competition Between Carbonation and Hydration on the Hardening of Calcium Hydroxide and Calcium Silicate Binders, 2009. PhD dissertation, KU Leuven.
[40] M. Arandigoyen, J.L.P. Bernal, M.A.B. López, J.I. Alvarez, Lime-pastes with different kneading water: Pore structure and capillary porosity, Appl. Surf. Sci. 252 (5) (2005) 1449–1459, https://doi.org/10.1016/j.apsusc.2005.02.145.
[41] D. Kralj, L. Brečević, Dissolution kinetics and solubility of calcium carbonate monohydrate, Colloids Surfaces A: Physicochem. Eng. Aspects 96 (3) (1995) 287–293, https://doi.org/10.1016/0927-7757(94), 03063-6.
[42] C. Rodriguez-Navarro, A. Suzuki, E. Ruiz-Agudo, Alcohol dispersions of calcium hydroxide nanoparticles for stone conservation, Langmuir 29 (36) (2013) 11457–11470, https://doi.org/10.1021/la4017728.
[43] V.S. Ramachandran, J.J. Beaudoin, Handbook of Analytical Techniques in Concrete Science and Technology: Principles Techniques and Applications, Noyes Publications, New Jersey, 2000.
[44] L. Fernández-Carrasco, D. Torrens-Martín, L.M. Morales, S. Martínez-Ramírez, Infrared spectroscopy in the analysis of building and construction materials, infrared spectroscopy - materials science, Eng. Technol. (2012), https://doi.org/10.5772/36186.
[45] P. Yu, R.J. Kirkpatrick, B. Poe, P.F. McMillan, X. Cong, Structure of calcium silicate hydrate (C-S-H): near-, mid-, and Far-Infrared Spectroscopy, J. Am. Ceram. Soc. 82 (3) (2004) 742–748, https://doi.org/10.1111/j.1151-2916.1999.tb01826.x.
[46] C. Fiori, M. Vandini, S. Prati, G. Chiavari, Vaterite in the mortars of a mosaic in the Saint Peter Basilica, Vatican (Rome), J. Cult. Herit. 10 (2) (2009) 248–257, https://doi.org/10.1016/j.culher.2008.07.011.
[47] R. Ševčík, P. Mácová, K. Sotiriadis, M. Pérez-Estébanez, A. Viani, P. Šašek, Micro-Raman spectroscopy investigation of the carbonation reaction in a lime paste produced with a traditional technology, J. Raman Spect. 47 (12) (2016) 1452–1457, https://doi.org/10.1002/jrs.4929.
[48] W. Kurdowski, in: Cement and Concrete Chemistry, Springer Science & Business, 2014, https://doi.org/10.1007/978-94-007-7945-7.
[49] L. Addadi, S. Raz, S. Weiner, Taking advantage of disorder: amorphous calcium carbonate and its roles in biomineralization, Adv. Mater. 15 (12) (2003), https://doi.org/10.1002/chin.200333237.
[50] J.J. Chen, J.J. Thomas, H.M. Jennings, Decalcification shrinkage of cement paste, Cem. Concr. Res. 36 (5) (2006) 801–809, https://doi.org/10.1016/j.cemconres.2005.11.003.